

Experiments and Molecular-Dynamics Simulation of Elastic Waves in a Plasma Crystal Radiated from a Small Dipole Source

A. Piel*

IEAP, Christian-Albrechts-Universität, D-24098 Kiel, Germany

V. Nosenko and J. Goree

Department of Physics and Astronomy, The University of Iowa, Iowa City, Iowa
(Received 27 December 2001; published 6 August 2002)

The radiation of elastic waves from a localized source is observed experimentally in a two-dimensional plasma crystal. An initial shear stress applied by a laser forms a small dipole source. The emerging complex wave pattern is shown to consist of outgoing compressional and shear wave pulses. Subsequent structures are identified as inward-going waves due to the finite size of the source region, which reappear on the opposite side. The compressional wave forms a trailing wave train due to strong dispersion, while the nondispersive shear wave evolves into a vortex-antivortex pair on either side. The experiments are compared with a molecular-dynamics simulation.

DOI: 10.1103/PhysRevLett.89.085004

PACS numbers: 52.27.Lw, 52.27.Gr, 52.35.Fp, 82.70.Dd

A crystalline lattice can vibrate with two kinds of sound waves, compressional and shear, with longitudinal and transverse polarization, respectively. In seismology these two wave types are called *P* and *S* waves, and their different propagation properties are used, e.g., to localize the epicenter of an earthquake or for geological exploration. The waves are usually excited by a localized pulsed source. Elastic waves are also used, e.g., to measure the Young modulus in thin diamondlike films [1]. The underlying physics of these waves is essentially the same in two-dimensional systems as in three dimensions. Therefore, we explore the radiation of such elastic waves from a small pulsed dipole source in a 2D Coulomb lattice (Wigner crystal), which is a convenient model solid. In such 2D lattices it is possible to study wave motion with video-microscopy of individual particle motion with *quasiatomic resolution*. This approach gives completely new insights for intricate cases of wave generation, propagation, and nonlinear interaction.

Plasma (Wigner) crystals [2–5] consist of a regular arrangement of micron-sized particles embedded in a gas discharge plasma. Under the influence of gravity flat monolayer (or multilayer) crystals are formed. Plane compressional waves in such systems were first excited with biased wires [6] and later with focused laser radiation [7,8]. Recently, plane shear wave pulses were generated with a rapidly scanning laser [9]. Supersonic objects [10,11] or a laser spot moving at supersonic velocity were used to excite compressional [12] and shear wave [13] Mach cones. The multiple structure of compressional Mach cones could recently be explained as an interference phenomenon caused by the dispersive nature of compressional waves [14].

While most of the earlier investigations were focused on the dispersion relation of plane waves and their diagnostic application, this Letter addresses the radiation problem

from a small localized source. The chosen geometry of a point-dipole source, is the most fundamental and can be considered as Green's function for more complicated situations. The experiments are compared with molecular-dynamics simulations in the same geometry. These observations contribute to the understanding of waves in the near field of an antenna that emits elastic waves.

Using apparatus similar to that described in Ref. [12] we suspend $8.1\ \mu\text{m}$ diameter polymer microspheres in an argon plasma with 15 mTorr pressure and 18 W rf power. They arrange themselves as a monolayer in a triangular lattice, which in our 24 mm by 18 mm field of view contains 990 particles with an average separation of 0.66 mm. The expanded beam of an argon-ion laser hits the plasma crystal at a small (10°) angle of incidence [Fig. 1(a)] and illuminates a nearly square spot of 4 mm by 4 mm size, where the laser force causes a localized shear stress that elastically deforms the crystal. The size of this region is chosen as a compromise between smallness and efficiency of wave excitation. Laser power (0.5 W) and laser pulse duration (250 ms) are chosen to avoid breaking bonds in the lattice.

In the *x* direction, the lattice is compressed ahead of the laser spot and rarefacted behind it, while in the *y* direction a symmetric shear stress is generated. The motion of the individual particles is recorded with a video camera (640×480 pixels) at 30 frames per second and a total of 32 frames. The experiment was repeated 100 times after 5.9 s recovery time each. The velocity field is calculated from particle positions with subpixel precision in subsequent video frames and interpolated to a fixed square grid for averaging. The velocity field during the laser pulse (frame 5) is shown in Fig. 1(b). It features a pronounced pair of elastic vortices of opposite sign. Although this velocity field resembles streamlines in fluids, there is no macroscopic flow but only a momentary elastic

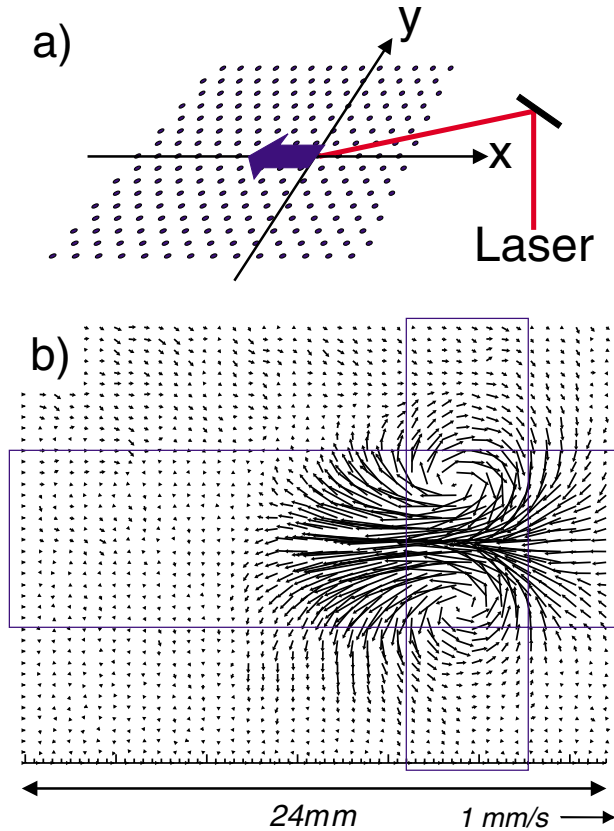


FIG. 1 (color online). (a) Geometry for localized elastic deformation of a 2D plasma crystal by a laser force. (b) Vector velocity map of particle motion during the laser pulse. The particle velocities have been interpolated to a square grid for averaging. The rectangles mark the stripes, which are used in subsequent figures to display the temporal evolution of shear and compressional wave.

deformation. After the end of the laser pulse, this elastic deformation relaxes and expands over a larger region than originally illuminated and is eventually radiated from the source region as a complex pattern of compressional and shear waves.

To understand the simultaneously occurring wave phenomena it is necessary to disentangle the two polarizations. In earlier investigations [12], the compressional wave was visualized in terms of a “numerical Schlieren map” by calculating the change in particle density $\partial n/\partial t$. Here we display the compressional wave by calculating the “divergence map” $\nabla \cdot \vec{v} = -(1/n)\partial n/\partial t$ which, in a linear approximation, is equivalent to the “Schlieren map” [12] because of conservation of particles. Similarly, we visualize the shear wave by the vorticity $\nabla \times \vec{v}$ of the velocity field. The vorticity is insensitive to compressional wave activity and the divergence of a shear wave is likewise negligible. In this way, independent information of the two wave modes is obtained. The rectangular stripes in Fig. 1(b) are the regions displayed in gray-scale maps of the shear wave [Fig. 2(a)] and compressional wave [Fig. 3(a)].

The initial situation for the shear wave in frame 2 of Fig. 2(a) shows a pair of vortices with opposite sign of vorticity. The positive and negative structures evolve in the $\pm y$ direction. This is the expected propagation direction for a plane shear wave, if the excitation region were extended in the x direction. Two pairs of lines are superimposed to guide the eye in tracing the propagation of the individual structures. In frame 8, the splitting of the structures into an outward- and inward-going wave pulse becomes evident. After a crossover of the inward-going waves in frame 10, these waves appear as outward-going waves in subsequent frames. The wave field eventually consists of two vortex-antivortex pairs propagating outwards. The leading vortex shows a stronger damping than the subsequent antivortex.

Double vortices form a class of particularly stable objects in hydrodynamics and in aerodynamics. It is a central result of these observations that the wave front of elastic shear waves consists of similar structures. Because of the weak dispersion of shear waves, the initially localized shear stress remains localized in the wave front, which is accomplished by forming a vortex-antivortex pair. This property may find applications, e.g., for optimizing the density of pulses in acoustical delay lines.

For the compressional wave [Fig. 3(a)] the situation is similar, but not identical. The initial pair, compression and rarefaction, in frame 0 propagates in the $\pm x$ direction. Again, the initial perturbation splits into ingoing and outgoing pulses. The ingoing pulses cross over in frame 2 and reappear as outward-going pulses in subsequent frames. Obviously the propagation speed for the compressional wave is higher than for the shear wave. The leading compressional pulse shows a stronger damping than the trailing rarefactive pulse. Wave damping is caused by neutral gas friction. While the wave field of the shear wave consists of only two pairs of vortices, the compressional wave

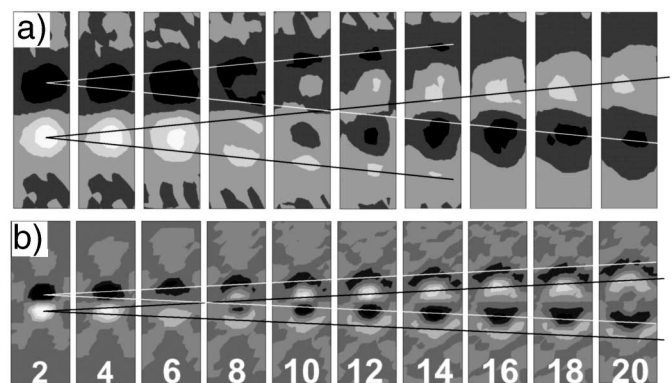


FIG. 2. Visualization of the shear wave in terms of the vorticity of the velocity field (black = cw, white = ccw). (a) Experiment; (b) molecular dynamics simulation. The stripes are 18 mm high. Time is indicated by the frame number (at 30 frames/s). Because of different values of κ the propagation speed in the simulation differs from the experiment.

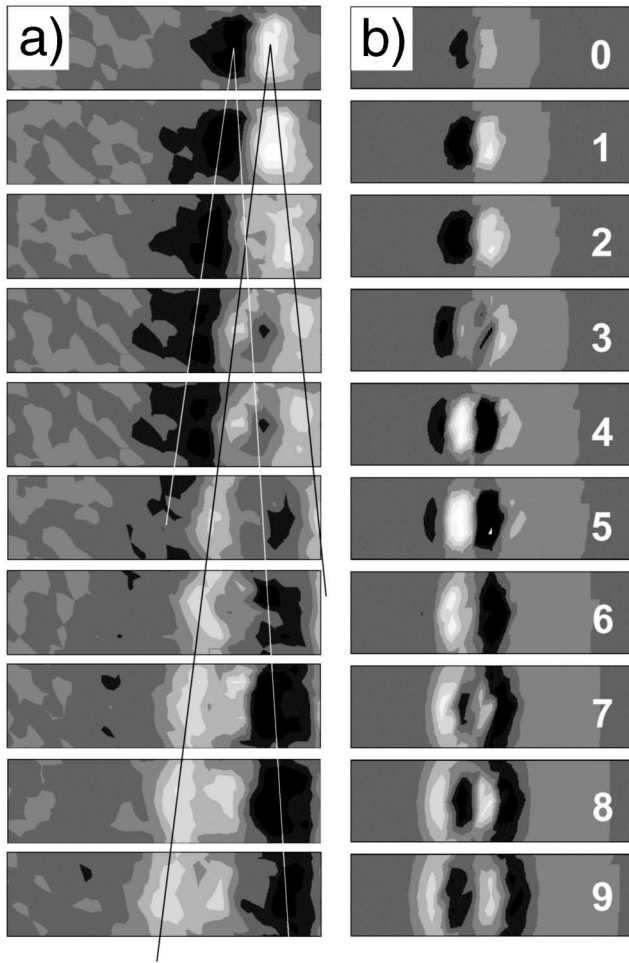


FIG. 3. Visualization of the compressional wave by the divergence of the velocity field (black = compression, white = rarefaction). (a) Experimental data; (b) molecular dynamics simulation. The stripes of 24 mm width are labeled by their frame number.

develops additional wave humps, as becomes evident from frames 7–9. We attribute this behavior to the larger dispersion of the compressional wave.

The sound speeds of compressional and shear wave are different for 2D crystals with Yukawa interaction potentials [15]. The ratio of the two sound speeds is a way to determine the shielding strength $\kappa = b/\lambda_D$, where b is the mean interparticle spacing and λ_D the Debye shielding length [12]. Here we find sound speeds of ($C_L = 24 \pm 2$) mm/s for the compressional wave and ($C_T = 7 \pm 1$) mm/s for the shear wave. From tabulated values of the sound speed ratio [16] we obtain $\kappa = 2.2 \pm 0.9$. This value is in accordance with earlier findings [7].

For comparison, we have performed molecular-dynamics simulations of localized wave excitation. The simulation starts with a regular triangular 2D crystal with $b = 0.75$ mm. The simulation area of 24 mm by 19.486 mm corresponds to 32 by 30 particles. The static lattice is continued with periodic boundary conditions in

four principal ($\pm x, \pm y$) and in four diagonal directions to confine the particles in the simulation box. The particles in the neighboring boxes are fixed, to avoid wave excitation in the exterior region. This approach allows studying the wave field until the faster wave reaches the boundary of the box, where it becomes reflected. The interparticle distance, the total number of particles (960), and the particle charge $Q = 14\,000e$ were chosen similar to the experimental conditions. The shielding factor $\kappa = 1$ was chosen for comparison with the theoretical dispersion curve in [14] and is lower than the experimental value, but the difference does not affect the topology of the wave modes, which is the major objective of this study. For immediate comparison with the experiment the simulation data are displayed as gray-scaled contour plots in Fig. 2(b) (shear wave) and Fig. 3(b) (compressional wave).

The simulation matches the experiment in several ways. The compressional and shear waves propagate in the $\pm x$ and $\pm y$ directions, respectively. The pulse splits into four features, and oppositely propagating features cross in the center. Only the compressional wave develops extra oscillations, attributable to dispersion, in frames 8 and 9. The damping for the leading pulse is stronger than for the following structure.

Our experimental and simulation results include not only the antenna's near field but its far field, where the wave fronts become circular. For the compressional wave the intensity distribution is inhomogeneous and resembles the $\cos^2\alpha$ distribution that is typical of dipole sources, and α is the angle with the x axis, while for the shear wave it is nearly $\sin^2\alpha$.

This topologically different behavior of compressional and shear waves can be further illuminated by a simple 1D model. Here we follow the evolution of an initially S-shaped perturbation. This structure is decomposed by fast Fourier transform into elementary waves $a(k, \omega)$, which are allowed to propagate according to their individual phase velocity $v_{ph}(k)$ in $\pm x$ direction. The dispersion of the compressional lattice wave is approximated by $\omega \simeq C_L k - Dk^3$ in the range $ka < 1$, with normalized coefficients $C_L = 2.44$ and $D = 0.67$ taken from Eqs. A7 and A9 in [14].

The shear wave has a nearly strictly acoustic dispersion $\omega = C_T k$. The result for the nondispersive wave is shown in Fig. 4(a), where the splitting of the positive and negative humps into right- and left-going pulses, crossover, and outgoing pairs of S-shaped structures is evident. In the case of the dispersive (compressional) wave [Fig. 4(b)], splitting and crossover of the original humps is seen again, but the dispersiveness of this wave leads to the formation of an oscillatory wave train. For typical conditions, the dispersion of this wave type is large enough to generate the additional humps seen in the experiment.

In summary, we have shown that the complex wave pattern from a localized, pulsed elastic stress applied to a plasma crystal can be decomposed into compressional and

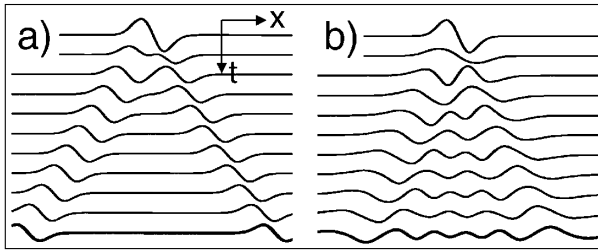


FIG. 4. 1D-model for pulse splitting and propagation (a) for the case of purely acoustic dispersion and (b) for the dispersion of a compressional wave. The horizontal scale extends over $x = \pm 32b$. The individual traces cover normalized times $\omega_{pd}t = 0-10$ where $\omega_{pd} = (Q_d^2/\epsilon_0 M_d b^3)^{1/2}$ is the dust plasma frequency and Q_d, M_d are the charge and mass of the particles.

shear waves, which eventually form spherical wave fronts. The intensity distribution of the two wave types is found dipolelike with orthogonal orientation. The finite size of the excitation region leads to the generation of additional inward-going waves, which cross at the center of the source region and reappear on the opposite side. The shear wave is found to be nondispersive, whereas the pronounced dispersion of the compressional wave leads to the formation of a wave train. A simple 1D model demonstrates that the dispersion is sufficiently large to explain the observed additional humps in our experiments. In our space-time measurement of the compressional wave the formation of a wave train is equivalent to the purely spatial interference structures found earlier inside the Mach cone of a compressional wave [12,14], which is absent in the less dispersive shear Mach cones [13]. Because of the weak dispersion, the initial shear stress in the excitation region remains confined to the wave front of the shear wave. This is accomplished by the formation of a vortex-antivortex pair. Theoretical studies of large Coulomb clusters [17] had shown earlier that the energetically lowest modes of excitation in confined systems of more than 100 particles are vortex-antivortex pairs. The spectra of large Yukawa clusters were recently studied in [18]. In the present investigations vortex-antivortex pairs are found as the building blocks of the wave front of shear waves. This is a further hint at the important role of double vortices for elastic waves.

One of the authors (A. P.) thanks DFG for the financial support under Grant No. Pi185/22-1 and gratefully acknowledges the hospitality experienced at the University of Iowa. TEM measurements of particle sizes were made by L. Boufendi (GREMI, Université d'Orléans). The work at Iowa was supported by NASA and DOE.

*Electronic address: piel@physik.uni-kiel.de

- [1] R. O. Dillon, A. Ali, N. Ianno, A. Ahmad, and T. Furtak, *J. Vac. Sci. Technol. A* **19**, 2826 (2001).
- [2] J. H. Chu and L. I, *Phys. Rev. Lett.* **72**, 4009 (1994).
- [3] H. Thomas, G.E. Morfill, V. Demmel, J. Goree, B. Feuerbacher, and D. Möhlmann, *Phys. Rev. Lett.* **73**, 652 (1994).
- [4] Y. Hayashi and K. Tachibana, *Jpn. J. Appl. Phys.* **33**, L804 (1994).
- [5] A. Melzer, T. Trottenberg, and A. Piel, *Phys. Lett. A* **191**, 301 (1994).
- [6] J. B. Pieper and J. Goree, *Phys. Rev. Lett.* **77**, 3137 (1996).
- [7] A. Homann, A. Melzer, S. Peters, and A. Piel, *Phys. Rev. E* **56**, 7138 (1997).
- [8] A. Homann, A. Melzer, S. Peters, R. Madani, and A. Piel, *Phys. Lett. A* **242**, 173 (1998).
- [9] S. Nunomura, D. Samsonov, and J. Goree, *Phys. Rev. Lett.* **84**, 5141 (2000).
- [10] D. Samsonov, J. Goree, Z. W. Ma, A. Bhattacharjee, H. M. Thomas, and G.E. Morfill, *Phys. Rev. Lett.* **83**, 3649 (1999).
- [11] D. Samsonov, J. Goree, H. M. Thomas, and G. E. Morfill, *Phys. Rev. E* **61**, 5557 (2000).
- [12] A. Melzer, S. Nunomura, D. Samsonov, Z. W. Ma, and J. Goree, *Phys. Rev. E* **62**, 4162 (2000).
- [13] V. Nosenko, J. Goree, Z. W. Ma, and A. Piel, *Phys. Rev. Lett.* **88**, 135001 (2002).
- [14] D. H. E. Dubin, *Phys. Plasmas* **7**, 3895 (2000).
- [15] F. M. Peeters and X. Wu, *Phys. Rev. A* **35**, 3109 (1987).
- [16] X. Wang, A. Bhattacharjee, and S. Hu, *Phys. Rev. Lett.* **86**, 2569 (2001).
- [17] V. A. Schweigert and F. Peeters, *Phys. Rev. B* **51**, 7700 (1995).
- [18] L. Candido, J.-P. Rino, N. Studart, and F. Peeters, *J. Phys. Condens. Matter* **10**, 11627 (1998).